Electronic, magnetic, and structural properties of CoVMnSb: ab initio study

Pavel V. Lukashev,^{1,*} Adam Ramker,¹ Brandon Schmidt,¹ Paul M. Shand,¹ Parashu Kharel,² Vagharsh Mkhitaryan,³ Zhenhua Ning,³ Liqin Ke³

¹Department of Physics, University of Northern Iowa, Cedar Falls, IA 50614, USA
²Department of Chemistry, Biochemistry, and Physics, South Dakota State University,
Brookings, SD 57007, USA
³Ames Laboratory, U.S. Department of Energy, Ames, Iowa 50011, USA

Abstract

We present computational results on electronic, magnetic, and structural properties of CoVMnSb, a quaternary Heusler alloy. Our calculations indicate that this material may crystallize in two energetically close structural phases: inverted and regular cubic. The inverted cubic phase is the ground state, with ferrimagnetic alignment, and around 80% spin polarization. Despite having a relatively large band gap in the minority-spin channel close to the Fermi level, this phase does not undergo a half-metallic transition under pressure. This is explained by the "pinning" of the Fermi level at the minority-spin states at Γ point. At the same time, the regular cubic phase is half-metallic, and retains its perfect spin polarization under a wide range of mechanical strain. Transition to regular cubic phase may be attained by applying uniform pressure (but not biaxial strain). In practice, this pressure may be realized by atomic substitution of non-magnetic atom (Sb) with another non-magnetic atom (Si) of smaller radius. Our calculations indicate that 25% substitution of Sb with Si results in half-metallic regular cubic phase being the ground state. In addition, CoVMnSb_{0.5}Si_{0.5} retains its half-metallic properties under a considerable range of mechanical pressure, as well as exhibits thermodynamic stability, thus making this alloy attractive for potential spintronic applications. We hope that the presented results will stimulate experimental efforts to synthesize this compound.

I. Introduction

The generation of highly spin-polarized current is one of the key aspects investigated for potential device applications in spin-based electronics (spintronics). In principle, the ideal material for such applications is a room temperature half-metal, i.e. a material that is conducting electrons of one spin only. 1,2,3,4,5,6,7,8,9,10,11,12,13 By definition, the spin-polarization (defined as P =

^{*} pavel.lukashev@uni.edu

 $\frac{N_{\uparrow}(\epsilon_F)-N_{\downarrow}(\epsilon_F)}{N_{\uparrow}(\epsilon_F)+N_{\downarrow}(\epsilon_F)}$ where $N_{\uparrow,\downarrow}(\epsilon_F)$ is the spin-dependent density of states (DOS) at the Fermi level, ϵ_F). ¹⁴ of half-metallic materials is 100%. At the same time, several physical mechanisms may reduce the spin-polarization of these compounds, thus destroying half-metallicity. In particular, atomic disorder almost always reduces the spin-polarization of potentially half-metallic materials. ^{15,16} In addition, surface states in reduced geometry (thin films) have been reported to have a negative impact on half-metallicity, by populating the energy band gap of one of the spin channels at the Fermi level. ^{17,18,19,20,21,22,23,24} At the same time, it has been reported that in some case, the half-metallicity in thin-film geometry may be restored by interface engineering. ^{25,26}

Among various materials that have been reported to exhibit half-metallic properties, such as certain oxides and manganites, ²⁷ double perovskites, ²⁸ chalcogenides, ²⁹ and pyrites, ³⁰ Heusler alloys attracted particular attention, mostly because they often have high Curie temperature, much higher than the room temperature. ^{31,32} Various types of Heusler compounds are distinguished. Semi-Heusler and full-Heusler alloys contain three and four atoms per formula unit, correspondingly. Full-Heusler compounds may be both ternary (A₂BC) and quaternary (ABCD). In addition, Heusler materials may crystallize in regular and inverted cubic structures. For example, the quaternary Heusler alloy ABCD has the following Wyckoff positions in the regular cubic structure: A(0,0,0), B(1/2,1/2,1/2), C(3/4,3/4,3/4), D(1/4,1/4,1/4). At the same time, in the inverted cubic structure, the Wyckoff positions are: A(0,0,0), B(3/4,3/4,3/4), C(1/2,1/2,1/2), D(1/4,1/4,1/4). Both structures have a symmetry of a space group F-43m, and are visualized in the Figure 1 below.

If the energy difference between the regular and inverted cubic phases of a Heusler compound is small, the material may, in principle, crystallize in either of the two phases. In addition, one of these phases may be half-metallic, while the other is not. For example, a ternary Heusler compound Ti₂MnAl exhibits 100% spin-polarization and spin-gapless semiconducting (SGS) electronic structure in inverted cubic phase, while in regular cubic phase this material is paramagnetic. ¹⁰ In such situations, it is important to understand how to stabilize the highly spin-polarized phase. This is the main topic of the current work.

CoVMnSb is a quaternary Heusler compound that has been recently reported to exhibit half-metallic properties.³³ Here, we show that the lowest energy state of this material (inverted cubic phase) is not half-metallic, and the transition of this phase to 100% spin polarization cannot

be induced by external strain. At the same time, under hydrostatic compression this material undergoes a transition to a regular cubic phase, which exhibits half-metallic electronic structure. Our calculations indicate that in practice such transition may be induced by substituting 25% of Sb atoms with Si, i.e. by "reducing" the atomic radius of the non-magnetic element.

The paper is organized as follows. The Computational Methods are described in Section II. Section III presents our main results, and it contains three sub-sections, which focus on the ground state properties of CoVMnSb, the effect of mechanical strain, and the effect of atomic substitution. Section IV contains concluding remarks and potential future work, and is followed by Acknowledgments and References to the relevant literature.

II. Computational methods

All calculations in this work are performed using the Vienna *ab initio* simulation package (VASP).³⁴ More specifically, the following methods are used: the projector augmented-wave method (PAW)³⁵ and generalized-gradient approximation (GGA) method by Perdew, Burke, and Ernzerhof, 36 as well as the integration method by Methfessel and Paxton with a 5×10^{-2} eV width of smearing.³⁷ The crystal structures are optimized until the energy difference between consecutive steps is 10^{-5} eV or less. The energy convergence criteria of 10^{-3} meV is used for calculating the electronic and magnetic structures. The Brillouin-zone integration is performed with a k-point mesh of $4\times4\times4$ for structural optimization, and $12\times12\times12$ for electronic structure calculations. The MedeA® software environment³⁸ is used for visualizing the atomic positions, and for calculating / plotting the electronic band structures. The ferromagnetic / ferrimagnetic alignments are modeled using supercell approach in VASP. More specifically, we relaxed the magnetic alignment to the lowest energy state in the 16-atom cell. The pair-exchange parameters from the Heisenberg Hamiltonian are calculated using in-house tight-binding code. The calculations reported in this work are performed using the Advanced Cyberinfrastructure Coordination Ecosystem: Services & Support (ACCESS) (formerly known as Extreme Science and Engineering Discovery Environment (XSEDE)) resources located at the Pittsburgh Supercomputing Center (PSC).³⁹, and with the local computer cluster at Ames National Laboratory.

III. Results

III. a) Ground state: structural, magnetic, and electronic properties

Figure 1 shows regular (a) and inverted (b) crystal structures of CoVMnSb, a quaternary Heusler alloy that has been recently reported to exhibit half-metallic electronic structure.³³ Our calculations indicate that this material has two energetically close lattice configurations: regular cubic, and inverted cubic. The calculated energies of these phases are -116.80110 eV / 16-atom cell, and -117.36817 eV / 16-atom cell, correspondingly. The calculated equilibrium lattice parameters are 5.997 Å for regular, and 6.131 Å for inverted structures.

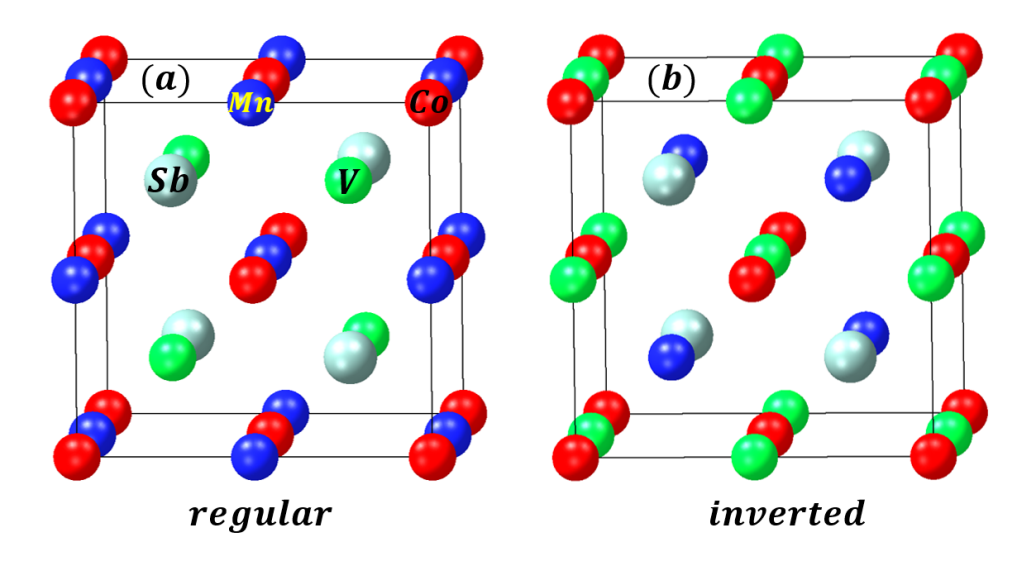


Figure 1: Regular (a) and inverted (b) crystal structure of CoVMnSb. The atoms are colored as indicated in the figure.

Figure 2 shows calculated density of states (DOS) of inverted (a) and regular (b) structures of CoVMnSb. The insets show the minority-spin states around Fermi level. As one can see, the inverted phase of this material is not half-metallic, due to the crossover of the spin-down states at the Fermi level. At the same time, slightly above the Fermi level, there is an energy gap of around 0.3 eV in the minority-spin channel. One may expect that the half-metallic transition may be induced in the inverted phase by shifting the Fermi level towards this energy gap by some external stimulus, e.g. by applying mechanical strain. Such transitions have been reported in literature for different Heusler compounds. At the same time, as one can see from Fig. 2 (b), the regular phase of CoVMnSb is half-metallic. Yet, a close inspection of the minority-spin states around the Fermi level reveals the potential absence of the energy gap. Instead, the half-metallicity appears

to be produced by a gapless character of these states (see the inset of Fig. 2 (b)). One may think that this makes the half-metallicity of the regular phase relatively unstable, as it may be destroyed e.g. by external pressure. Thus, for both the regular and inverted phases of CoVMnSb, it is desirable to analyze the effect of external pressure on their electronic structure. This question is addressed in detail in the next section.

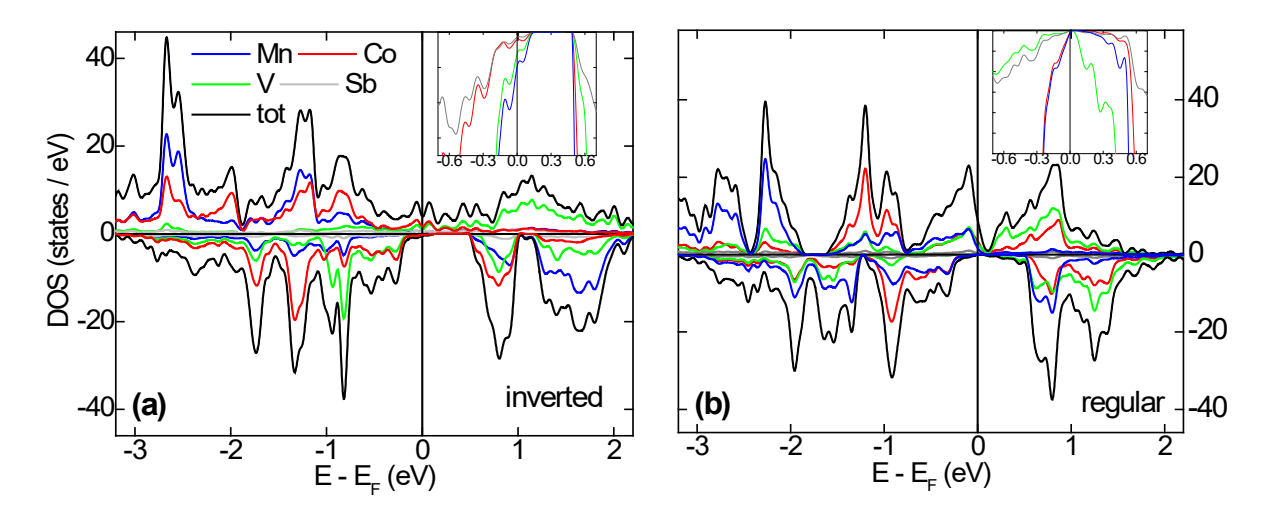


Figure 2: Calculated total and element-resolved density of states of inverted (a) and regular (b) phases of CoVMnSb. Elemental contributions are colored as indicated in the figure. Positive DOS corresponds to the majority-spin states, while negative DOS corresponds to the minority-spin states. The vertical line indicates position of the Fermi level. The insets show the distribution of the spin-down states around the Fermi energy.

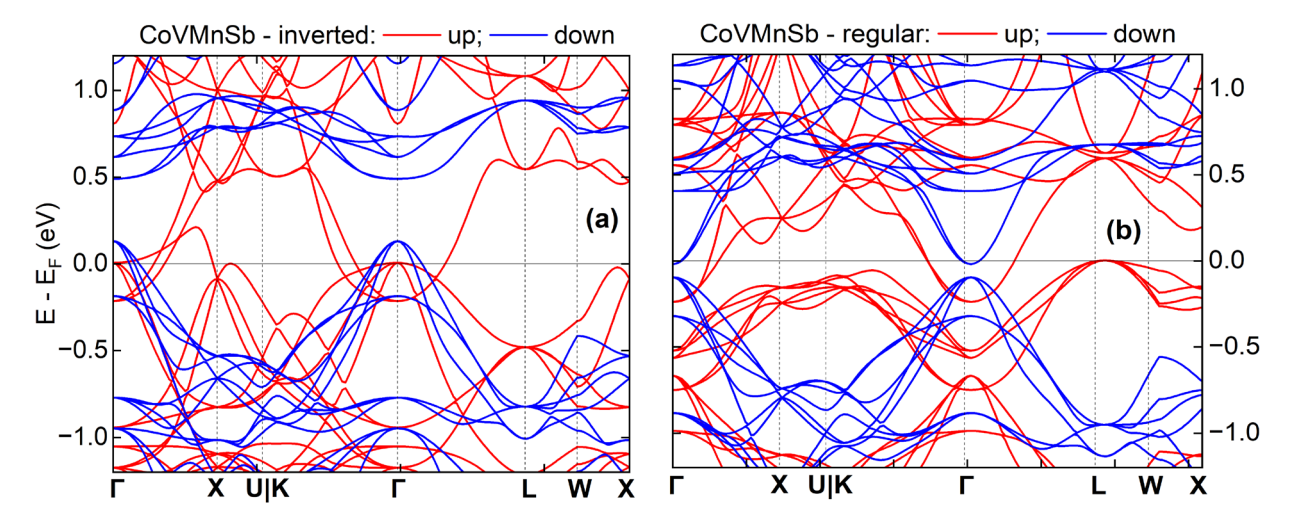


Figure 3: Calculated band structure of inverted (a) and regular (b) phases of CoVMnSb. Blue: minority-spin bands; red: majority-spin bands. Horizontal line is the middle of the plot corresponds to the Fermi level.

Figure 3 shows calculated band structure of inverted (a) and regular (b) phases of CoVMnSb (blue and red line indicate minority- and majority- spin bands, correspondingly). As one can see from Fig. 3 (b), the minority-spin states actually *do* exhibit an energy gap around the Fermi level, but its value is fairly small (around 0.1 eV). This gap is not visible in the Fig. 2 (a) due to the non-zero smearing of the DOS plot. Either way, both the Figures 2 and 3 confirm the half-metallic nature of the regular phase, and non-half-metallic (but still highly spin-polarized) nature of the inverted phase of CoVMnSb. More specifically, the values of the spin-polarization (calculated using $P = \frac{N_{\uparrow}(\epsilon_F) - N_{\downarrow}(\epsilon_F)}{N_{\uparrow}(\epsilon_F) + N_{\downarrow}(\epsilon_F)}$ where $N_{\uparrow,\downarrow}(\epsilon_F)$ is the spin-dependent density of states at the Fermi level, ϵ_F) are 98.9% and 80.2% for the regular and inverted phases, correspondingly. A small deviation of the spin-polarization of the regular phase from 100% is likely due to the DOS smearing. As shown at the band structure plot (Fig. 3 (b)), the regular phase of CoVMnSb is half-metallic.

	Total (µ _B / f.u.)	Co (µ _B / atom)	Mn (µ _B / atom)	V (μ _B / atom)	Sb (μ_B / atom)
regular	2.000	1.195	0.292	0.531	-0.018
inverted	2.018	0.786	3.162	-1.735	-0.034

Table 1: Calculated magnetic moments (total, and atom-resolved) of both inverted and regular structures of CoVMnSb at equilibrium.

Table 1 shows calculated magnetic moments (total, and atom-resolved) of both inverted and regular structures of CoVMnSb at equilibrium. Interestingly, these two phases exhibit distinctly different magnetic alignment. In particular, as one can see from Table 1, CoVMnSb is ferromagnetic in its regular phase, and ferrimagnetic in the inverted phase. The ferrimagnetic alignment in the inverted structure results from the magnetic moment of vanadium being antialigned with the magnetic moments of cobalt and manganese. At the same time, the total magnetic moments of these two phases are relatively close, due to a much larger (order of magnitude) value of Mn magnetic moment in the inverted phase. Another noteworthy feature of the data presented in Table 1 is the integer (non-integer) value of the total magnetic moment of CoVMnSb in the regular (inverted) phase. This is consistent with our conclusion that CoVMnSb is half-metallic in the regular phase, but not half-metallic in the inverted phase. In particular, the integer magnetic moment per formula unit may serve as an indication of half-metallicity. Indeed, in the case of half-moment per formula unit may serve as an indication of half-metallicity. Indeed, in the case of half-

metallic electronic structure (see Figures 2(b) and 3 (b)), the spin-down states in the valence band are fully occupied, thus making their total number an integer. This results in an integer total magnetic moment per formula unit, because the total valence charge is an integer.

To confirm the ferrimagnetic alignment of the inverted phase, we computed exchange coupling parameters (J_{ij}) between vanadium atoms and their neighbors in both regular and inverted structures. These calculations were conducted using an in-house tight-binding code, 41,42 employing the linear response theory 43 and the maximally localized Wannier functions (MLWFs) method. 44,45,46 MLWFs have the capability to represent either an isolated set of bands or entangled bands within a specified energy range using a more compact basis. The linear response method calculates individual pair couplings (J_{ij}) by assessing energy variations resulting from infinitesimal spin rotations of atoms i and j, utilizing the magnetic force theorem. Positive values of pair-exchange parameters J_{ij} indicate antiferromagnetic alignment, while negative values of J_{ij} indicate ferromagnetic alignment.

The calculated J_{ij} parameters are plotted in the Figure 4. Here, the abscissa indicates the nearest neighbor (x=1), next nearest neighbor (x=2), and so on. The pairs that are not shown in the figure (V - Sb in both structures, and V - V in regular structure) have negligible value of J_{ij} .

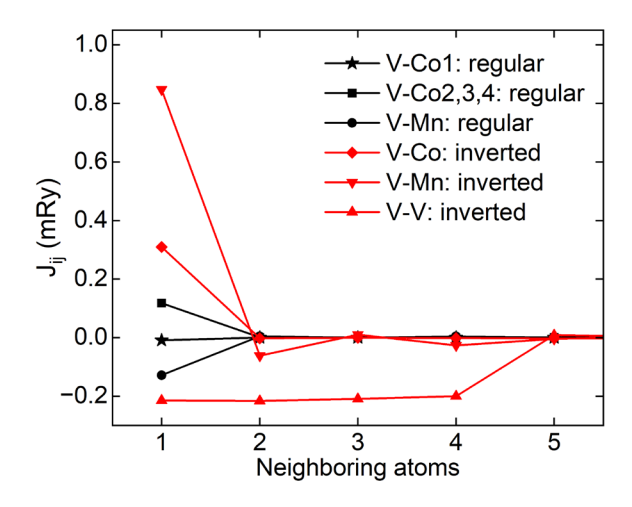


Figure 4: Calculated pair-exchange parameters, J_{ij} between vanadium atom and its neighbors in both regular (black) and inverted (red) structures of CoVMnSb. Different symbols are used to represent different pairs, as indicated in the figure.

One of the main features seen in Fig. 4 is a strong positive exchange coupling between nearest neighbor V and Mn atoms in inverted structure (red triangles facing down). The positive

value of J_{ij} indicates antialigned magnetic moments of V and Mn in inverted structure. The exchange coupling between V and Co atoms in inverted structure (red rhombuses) is also positive, again favoring antialignment of V and Co magnetic moments. At the same time, the exchange coupling between two V atoms is negative, which results in magnetic moments of vanadium atoms pointing in the same direction. In the regular structure, the magnetic moment of V is around three times smaller than that in the inverted structure. This results in much smaller $|J_{ij}|$ values in the regular structure compared with inverted structure, as can be seen in Fig. 4. In addition, the exchange coupling between nearest neighbor V and Mn atoms in regular structure (black solid circles) is negative, indicating ferromagnetic alignment. Finally, the exchange coupling between nearest neighbor V and Co atoms in regular structure may be both positive (black solid squares) and around zero (black stars). The zero value of J_{ij} may be a computational artifact, as it is only observed in one out of four V – Co nearest neighbors. For the other three V – Co pairs, J_{ij} is positive. This should result in antialignment of V and Co magnetic moment in regular structure, which is not confirmed by our calculations (see Table 1). This is likely due to the negative J_{ij} value for all four nearest neighbor V and Mn pairs. In other words, the tendency towards alignment between V and Mn magnetic moments appears to outweigh the tendency towards antialignment between V and Co magnetic moments, in the regular structure.

We also estimated the Curie temperature of CoVMnSb in the regular cubic (half-metallic) phase within the mean field approximation, as follows: $T_c = \frac{2||E_{FM}| - |E_{AFM}||}{3nk_B}$. ^{47,48} Here, n is the number of magnetic atoms in the cell (12, in our case), while $E_{FM} = -116.801902 \ eV$ and $E_{AFM} = -116.150385 \ eV$ are calculated energies of ferromagnetic and antiferromagnetic arrangements, correspondingly. The calculated value of T_c is 421 K, i.e. much higher than room temperature. Moreover, the calculated values of E_{FM} and E_{AFM} confirm the stability of the ferromagnetic phase.

III. b) Mechanical strain: structural, magnetic, and electronic properties

As discusses in the previous sub-section, the properties of both the regular and inverted phases of CoVMnSb may be very sensitive to the external pressure. Figure 5 shows calculated energies of these phases as a function of lattice constant for uniform (hydrostatic) pressure (a), and biaxial strain (b). Here, the biaxial strain is modeled as follows: for each of the considered in-plane

lattice parameters, we optimized the out-of-plane lattice parameter. The calculated out-of-plane vs. in-plane lattice constants (c vs. a) for both the regular and inverted phases of CoVMnSb are plotted in the Fig. 5 (c).

As seen from the Fig. 5 (a), application of the uniform pressure leads to the regular phase of CoVMnSb becoming a lower energy state compared with the inverted phase. The transition happens at the lattice constant of 5.981 Å. At the same time, application of the biaxial strain does not result in such a transition (see Fig. 5 (b)), likely due to a smaller change of the unit cell volume. In principle, biaxial strain is a more realistic scenario of modifying the volume of the unit cell. In particular, it can be induced in thin-film geometry, by growing the material on a substrate with a different lattice constant. At the same time, the hydrostatic pressure may also be induced in practice, e.g. by atomic substitution. For example, in our recent work we demonstrated that atomic substitution induced reduction of the unit cell volume leads to a half-metallic transition in a semi-Heusler compound CrMnSb. ⁴⁹ Therefore, in the rest of this paper we focus on the effect of hydrostatic pressure, as it may potentially result in a half-metallic transition, due to the regular phase of CoVMnSb becoming the ground state.

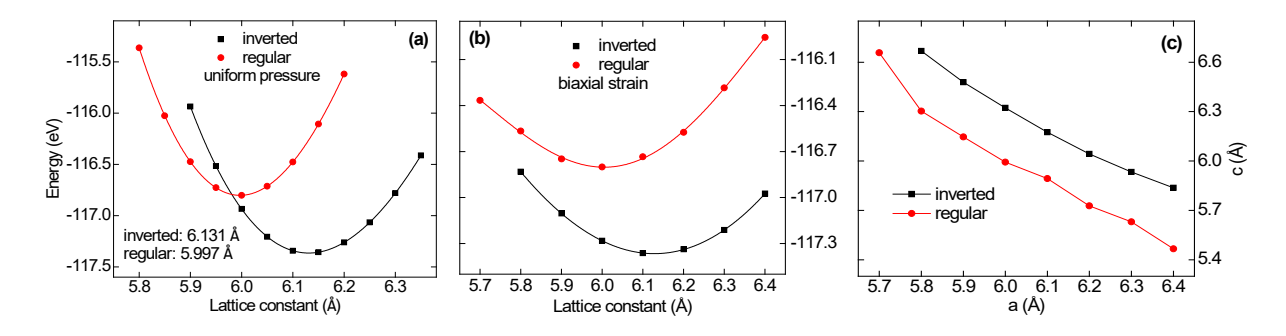


Figure 5: Calculated energies of the inverted (black line and squares) and regular (red line and circles) phases of CoVMnSb as a function of lattice constant for uniform (hydrostatic) pressure (a) and biaxial strain (b). Calculated out-of-place vs. in-plane lattice constant (c vs. a) of the inverted (black line and squares) and regular (red line and circles) phases of CoVMnSb (c).

Next, we analyze how the electronic and magnetic properties of CoVMnSb change under applied uniform pressure. Figure 6 shows calculated spin polarization (a) and magnetization (b) of the inverted (black line and squares) and regular (red line and circles) phases of CoVMnSb under uniform pressure, as a function of lattice constant. One can see that under compression the regular phase essentially retains its 100% spin polarization and integer value of the magnetic moment, except maybe at the largest considered compression (a=5.800 Å). Interestingly, under expansion

(negative pressure), the spin polarization of the regular phase strongly decreases and eventually changes sign. At the same time, the behavior of the spin polarization and magnetization of the inverted phase does not indicate any tendency towards half-metallic transition under uniform pressure. To understand these trends better, we next analyze the evolution of the electronic structure of CoVMnSb under uniform pressure.

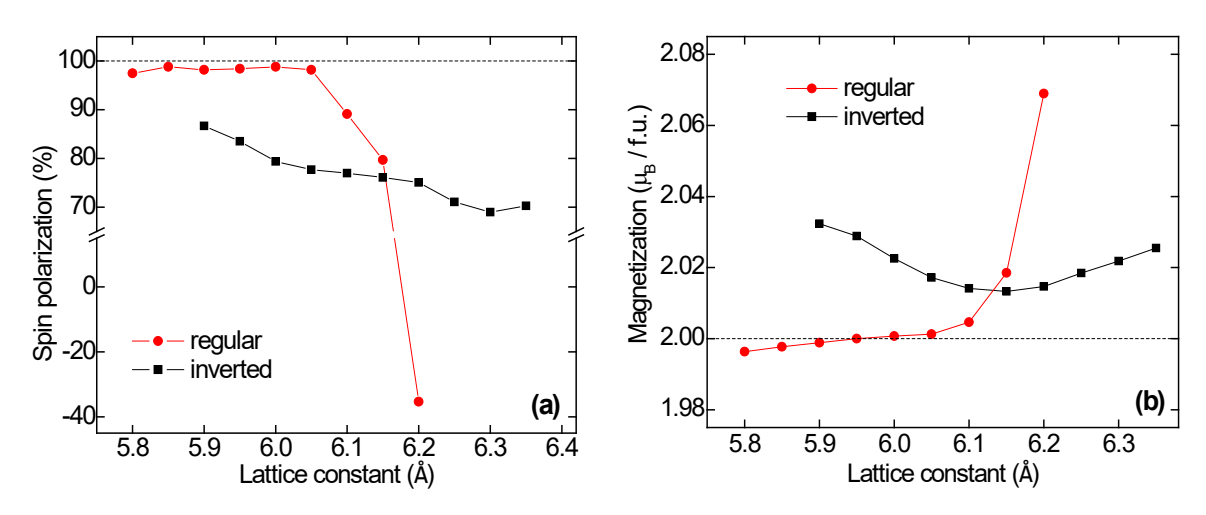


Figure 6: Calculated spin polarization (a) and magnetization (b) of the inverted (black line and squares) and regular (red line and circles) phases of CoVMnSb under uniform pressure, as a function of lattice constant.

Figure 7 shows calculated total density of states of the regular (a) and inverted (b) phases of CoVMnSb under uniform pressure, as a function of lattice constant. The calculated spin polarization values, as well as the lattice parameters at which DOS is calculated are shown in the figure. One can see that except for the two largest considered lattice constants of the regular phase (where the half-metallicity is apparently destroyed), the DOS profile stays relatively insensitive to the external pressure for both the inverted and regular phases. This is a rather interesting behavior, with the following two implications: first, if the regular phase of CoVMnSb is stabilized, e.g. by applying pressure to this alloy, it should retain its half-metallic properties in the considered range of the lattice parameters ($\sim 5.800-6.000 \text{ Å}$). At the same time, it appears that the half-metallic transition in the inverted phase cannot be induced by external pressure.

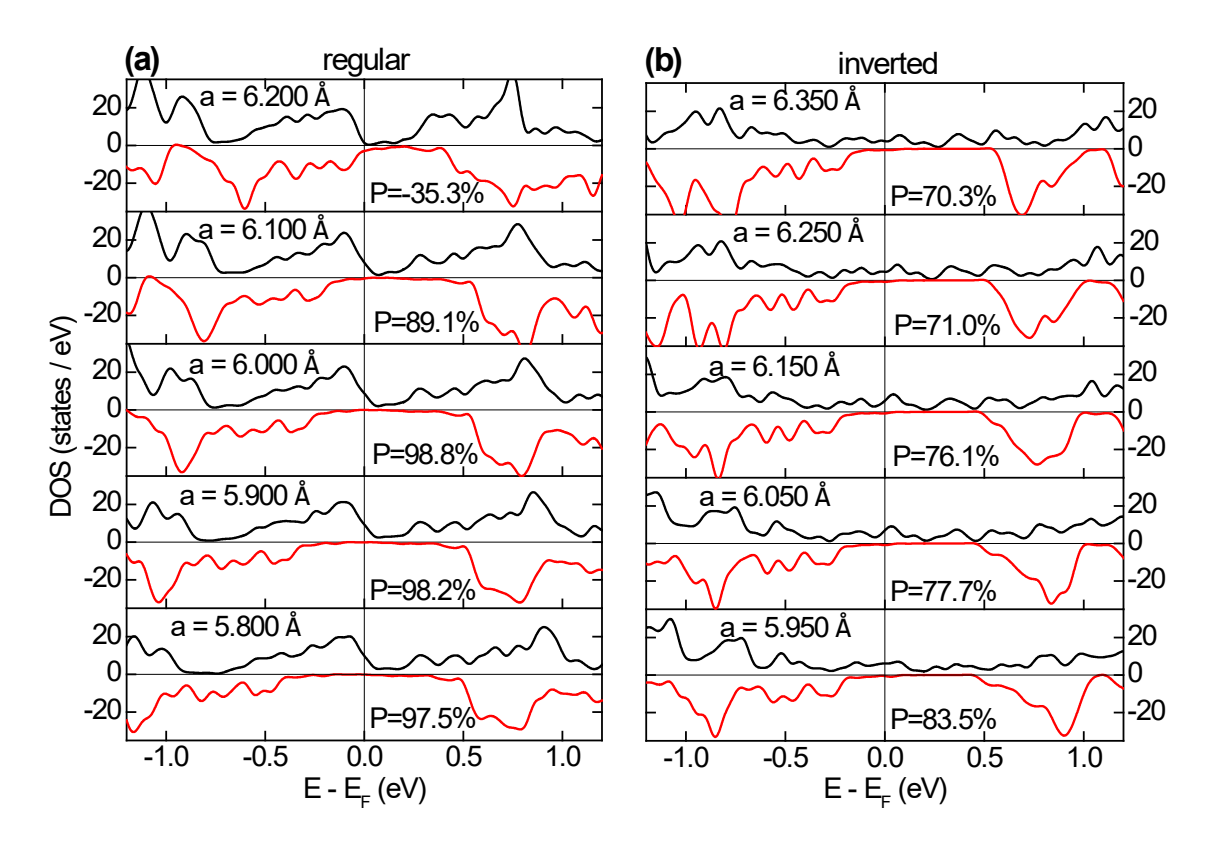


Figure 7: Calculated total density of states of the regular (a) and inverted (b) phases of CoVMnSb under uniform pressure, as a function of lattice constant. The calculated spin polarization values, as well as the lattice parameters at which DOS is calculated are shown in the figure. Black line / positive DOS corresponds to the majority-spin channel, red line / negative DOS corresponds to the minority-spin channel.

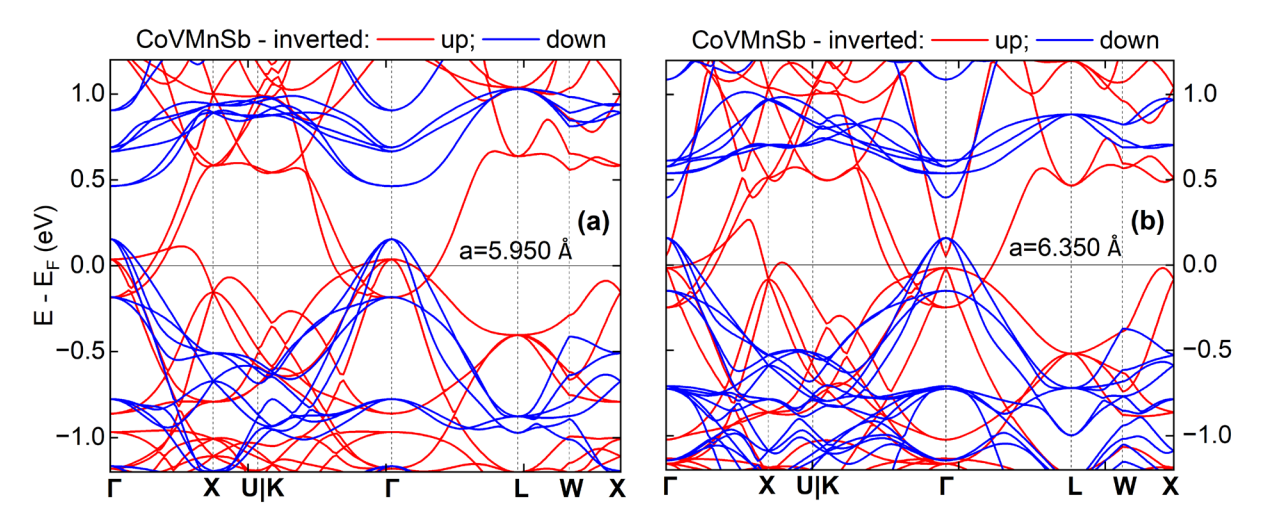


Figure 8: Calculated band structure of the inverted phase of CoVMnSb at a=5.950 Å (a) and at a=6.350 Å (b). Blue: minority-spin bands; red: majority-spin bands. Horizontal line is the middle of the plot corresponds to the Fermi level.

As discussed above, it is not immediately clear from the DOS plots, why the spin polarization of the inverted phase is so low. In particular, on the scale shown in the Figure 7 (b), it may appear that the Fermi level is actually positioned in the minority-spin energy gap. To illustrate that this is not so, we also plot the band structure of the inverted phase of CoVMnSb under compression and under expansion, see Figure 8. One can see that the bands of the inverted phase are not very sensitive to the change of the unit cell volume (compare Fig. 8 (a) and (b) with Fig. 3 (a)). In particular, the minority-spin bands (blue line) cross the Fermi level at the Γ point in all three considered regimes (compression, expansion, equilibrium). This explains the absence of the half-metallic transition of the inverted phase of CoVMnSb under pressure.

III. c) Atomic substitution: CoVMnSb_{0.75}Si_{0.25}

As discussed above, at the lattice constant of 5.981 Å (and smaller), the regular phase of CoVMnSb becomes the energetically favorable structure (see Fig. 5 (a)). A realistic way to reduce the unit cell volume is to substitute some of the larger radius atoms with smaller radius atoms. To model this scenario, we replaced 25% of antimony with silicon in both the regular and inverted phases, i.e. we replaced one out of four Sb atoms with Si in a 16-atom cell. The calculated energies, lattice parameters, and spin polarizations of CoVMnSb_{0.75}Si_{0.25} after structural optimization are listed in Table 2. One can see that the regular phase of CoVMnSb_{0.75}Si_{0.25} has lower energy than the inverted phase. In addition, the regular phase retains its nearly 100% spin polarization, while the spin polarization of the inverted phase is only around 66%. Thus, we conclude that the substitution of 25% of Sb with Si in results in CoVMnSb results in a half-metallic transition.

	Energy (eV / 16-atom cell)	lattice constant (Å)	spin polarization (%)
regular	-119.67428	5.914	98.1
inverted	-119.62723	6.041	66.3

Table 2: Calculated energies, lattice parameters, and spin polarizations of CoVMnSb_{0.75}Si_{0.25} after structural optimization.

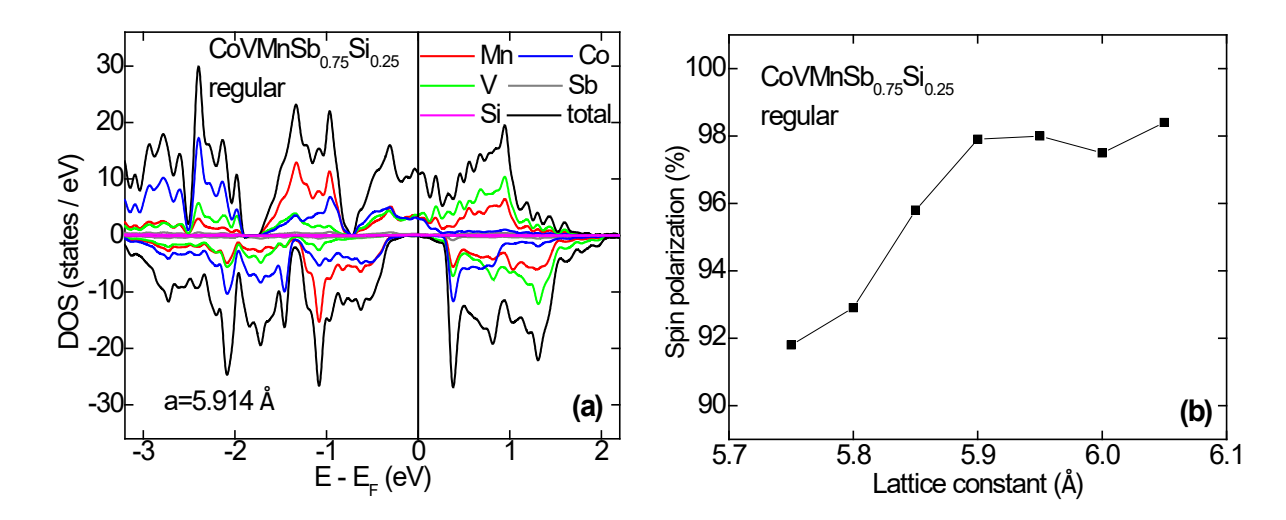


Figure 9: (a) Calculated total and element-resolved density of states of the regular phase of CoVMnSb_{0.75}Si_{0.25}. Elemental contributions are colored as indicated in the figure. Positive DOS corresponds to the majority-spin states, while negative DOS corresponds to the minority-spin states. The vertical line indicates position of the Fermi level. (b) Calculated spin polarization of the regular phase of CoVMnSb_{0.75}Si_{0.25} under uniform pressure, as a function of lattice constant.

Figure 9 shows calculated density of states of CoVMnSb_{0.75}Si_{0.25} at equilibrium (a), and calculated spin polarization of CoVMnSb_{0.75}Si_{0.25} under hydrostatic pressure as a function of lattice constant (b). Fig. 9 (a) confirms the half-metallic electronic structure of this alloy. In addition, as one can see from Fig. 9 (b), CoVMnSb_{0.75}Si_{0.25} retains a large spin polarization (over 90%) in the entire range of the considered lattice parameters, thus making it attractive for potential practical applications in spin-based electronic devices.

Finally, we estimated the formation energy of CoVMnSb_{0.75}Si_{0.25} as follows:

$$E_{form} = E(Co_4V_4Mn_4Sb_3Si_1) - 4E(Co) - 4E(Mn) - 4E(V) - 3E(Sb) - E(Si) \rightarrow$$

$$E_{form} = -1.864~eV$$

Here, E_{form} is the formation energy of CoVMnSb_{0.75}Si_{0.25}, $E(Co_4V_4Mn_4Sb_3Si_1)$ is the calculated total energy of bulk CoVMnSb_{0.75}Si_{0.25} (16-atom cell) in a regular cubic phase, while E(Co), E(Mn), E(V), E(Sb), and E(Si) are the corresponding total energies per atom of the listed bulk elements. The negative value of E_{form} indicates potential thermodynamic stability of CoVMnSb_{0.75}Si_{0.25}. Therefore, we foresee experimental efforts in synthesizing this alloy as a future direction of this research.

IV. Conclusions

Here, we presented results of a comprehensive first-principles study of a quaternary Heusler compound, CoVMnSb. It is shown that this alloy may crystallize in two energetically close cubic crystal structures, regular and inverted. The cubic regular structure is half-metallic, however, in a stoichiometric phase, the inverted structure has lower energy, and it exhibits reduced spin-polarization of around 80%. In addition, despite having a sizable energy gap in the minority-spin channel close to the Fermi level, the inverted phase does not exhibit a half-metallic transition, e.g. under external mechanical strain. Instead, the half-metallic transition in CoVMnSb may be induced by a hydrostatic pressure, i.e. by reducing the volume of the unit cell, when the regular cubic phase becomes the ground state. In practice, this reduction may be achieved by atomic substitutions of a non-magnetic element (Sb) with another non-magnetic element (Si) of a smaller atomic radius. More specifically, our calculations indicated that CoVMnSb_{0.75}Si_{0.25} exhibits ground state half-metallicity in a considerable range of lattice parameters. In addition, we confirmed the thermodynamic stability of this material by estimating its formation energy. We hope that these results may stimulate experimental efforts to synthesize this alloy, which may have practical applications in the field of spin-based electronics.

Data availability statement

The data that support the findings of this study are available from the corresponding author upon reasonable request.

Acknowledgments

This research is supported by the *US Department of Energy* (DOE) Visiting Faculty Program (VFP) at the Ames National Laboratory, and by the *National Science Foundation* (NSF) under Grant Numbers 2003828 and 2003856 via DMR and EPSCoR. This work used the Advanced Cyberinfrastructure Coordination Ecosystem: Services & Support (ACCESS) (formerly known as Extreme Science and Engineering Discovery Environment (XSEDE)), which is supported by National Science Foundation grant number ACI-1548562. This work used the XSEDE Regular

Memory (Bridges 2) and Storage (Bridges Ocean) at the Pittsburgh Supercomputing Center (PSC) through allocation TG-DMR180059.

References

¹ R. A. de Groot, F. M. Mueller, P. G. van Engen, and K. H. J. Buschow, Phys. Rev. Lett. **50**, 2024 (1983).

² I. Galanakis, P. H. Dederichs, and N. Papanikolaou, Phys. Rev. B **66**, 174429 (2002).

E. Şaşıoğlu, L. M. Sandratskii, P. Bruno, and I. Galanakis, Phys. Rev. B 72, 184415 (2005).

⁴ S. Picozzi, A. Continenza, and A. J. Freeman, Phys. Rev. B **66**, 094421 (2002).

⁵ B. Balke, G. H. Fecher, J. Winterlik, and C. Felser, Appl. Phys. Lett. **90**, 152504 (2007).

⁶ H. Kurt, K. Rode, M. Venkatesan, P. Stamenov, and J. M. D. Coey, Phys. Status Solidi B **248**, 2338 (2011).

⁷ J. Winterlik, S. Chadov, A. Gupta, V. Alijani, T. Gasi, K. Filsinger, B. Balke, G. H. Fecher, C. A. Jenkins, F. Casper, J. Kübler, G. Liu, L. Gao, S. S. P. Parkin, C. Felser, Adv. Mater. **24**, 6283 (2012).

⁸ A. Nelson, P. Kharel, Y. Huh, R. Fuglsby, J. Guenther, W. Zhang, B. Staten, P. Lukashev, S. Valloppilly, and D. J. Sellmyer, J. Appl. Phys. **117**, 153906 (2015).

⁹ I. Galanakis, Heusler Alloys (Springer Series in Materials Science, vol. 222) ed. C. Felser and A. Hirohata (Berlin: Springer, 2016).

P. Lukashev, P. Kharel, S. Gilbert, B. Staten, N. Hurley, R. Fuglsby, Y. Huh, S. Valloppilly, W. Zhang, K. Yang, R. Skomski, and D. J. Sellmyer, Appl. Phys. Lett. 108, 141901 (2016).

I. Tutic, J. Herran, B. Staten, P. Gray, T. R. Paudel, A. Sokolov, E. Y. Tsymbal, and P. V. Lukashev, J. Phys.: Condens. Matter 29, 075801 (2017).

¹² J. Herran, R. Carlile, P. Kharel, and P. Lukashev, J. Phys.: Condens. Matter **31**, 495801 (2019).

¹³ S. Prophet, R Dalal, P. Kharel, and P. Lukashev, J. Phys.: Condens. Matter 31, 055801 (2019).

¹⁴ J. P. Velev, P. A. Dowben, E. Y. Tsymbal, S. J. Jenkins, and A. N. Caruso, Surf. Sci. Rep. **63**, 400 (2008).

P. Kharel, J. Herran, P. Lukashev, Y. Jin, J. Waybright, S. Gilbert, B. Staten, P. Gray, S. Valloppilly, Y. Huh, and D. J. Sellmyer, AIP Advances 7, 056402 (2017).

¹⁶ P. Lukashev, Z. Lehmann, L. Stuelke, R. Filippone, B. Dahal, S. Valloppilly, J. Waybright, A. Pathak, Y. Huh, P. Shand, P. Kharel, J. Alloys. Compd. **895**, 162625 (2022).

¹⁷ F.B. Mancoff, B.M. Clemens, E.J. Singley, D.N. Basov, Phys. Rev. B **60**(R12) 565 (1999).

¹⁸ G. Bona, F. Meier, M. Taborelli, E. Bucher, P. Schmidt, Solid State Commun. **56**, 391 (1985).

¹⁹ W. Zhu, B. Sinkovic, E. Vescovo, C. Tanaka, J.S. Moodera, Phys. Rev. B **64**, R060403 (2001).

²⁰ A.N. Caruso, C.N. Borca, D. Ristoiu, J.P. Nozieres, P.A. Dowben, Surf. Sci. **525**, L109 (2003).

D. Ristoiu, J.P. Nozières, C.N. Borca, B. Borca, P.A. Dowben, Appl. Phys. Lett. 76, 2349 (2000).

²² I. Galanakis, J. Phys. Condens. Matter **14**, 6329 (2002).

²³ I. Galanakis, J. Magn. Magn. Mater. **288**, 411 (2005).

²⁴ M. Ležaic, I. Galanakis, G. Bihlmayer, S. Blügel, J. Phys. Condens. Matter 17, 3121 (2005).

²⁵ G. Wijs, R. de Groot, Phys. Rev. B **64**, R020402 (2001).

²⁶ A. Debernardi, M. Peressi, A. Baldereschi, Mater. Sci. Eng. C-Bio. S 23, 743 (2003).

²⁷ R.J. Soulen Jr, J.M. Byers, M.S. Osofsky, B. Nadgorny, T. Ambrose, S.F. Cheng, P.R. Broussard, C.T. Tanaka, J. Nowak, J.S. Moodera, A. Barry, J.M.D. Coey, Science **282**, 85 (1998).

²⁸ H. Kato, T. Okuda, Y. Okimoto, Y. Tomioka, K. Oikawa, T. Kamiyama, Y. Tokura, Phys. Rev. B 69, 184412 (2004).

M. Horne, P. Strange, W.M. Temmerman, Z. Szotek, A. Svane, H. Winter, J. Phys. Condens. Matter 16, 5061 (2004)

³⁰ T. Shishidou, A.J. Freeman, R. Asahi, Phys. Rev. B **64**, 180401 (2001).

- P.J. Webster, K.R.A. Ziebeck, in *Alloys and Compounds of d-Elements with Main Group Elements*. Part 2. Landolt-Börnstein, New Series, Group III, vol 19c, ed. by H.R.J. Wijn (Springer, Berlin 1988) pp. 75–184.
- ³² J. Kübler, Phys. Rev. B **67**, 220403 (2003).
- ³³ H. Zhou, H. Huang, and S. Luo, Phys. Solid State, **63** (2), 272 (2021).
- ³⁴ G. Kresse and D. Joubert, Phys. Rev. B **59**, 1758 (1999).
- ³⁵ P. Blöchl, Phys. Rev. B **50**, 17953 (1994).
- ³⁶ J. P. Perdew, K. Burke, and M. Ernzerhof, Phys. Rev. Lett. **77**, 3865 (1996).
- ³⁷ M. Methfessel and A. T. Paxton, Phys. Rev. B **40**, 3616 (1989).
- ³⁸ MedeA-2.22, Materials Design, Inc., San Diego, CA, USA, 2017.
- J. Towns, T. Cockerill, M. Dahan, I. Foster, K. Gaither, A. Grimshaw, V. Hazlewood, S. Lathrop, D. Lifka, G. D. Peterson, R. Roskies, J. R. Scott, N. Wilkins-Diehr, "XSEDE: Accelerating Scientific Discovery", Computing in Science & Engineering, vol.16, no. 5, pp. 62-74, Sept.-Oct. 2014.
- ⁴⁰ I. Galanakis, P. H. Dederichs, N. Papanikolaou, Phys. Rev. B **66**, 134428 (2002).
- ⁴¹ L. Ke, Phys. Rev. B **99**, 054418 (2019).
- ⁴² Z. Ning, B. Li, A. Banerjee, V. Fanelli, D. Abernathy, Y. Liu, B. Ueland, R. McQueeney, and L. Ke (in preparation).
- ⁴³ A. Liechtenstein, M. Katsnelson, V. Antropov, and V. Gubanov, J. Magn. Magn. Mater. **67**, 65 (1987).
- ⁴⁴ N. Marzari and D. Vanderbilt, Phys. Rev. B **56**, 12847 (1997).
- ⁴⁵ N. Marzari, A. Mostofi, J. Yates, I. Souza, and D. Vanderbilt, Rev. Mod. Phys. **84**, 1419 (2012).
- ⁴⁶ I. Souza, N. Marzari, and D. Vanderbilt, Phys. Rev. B **65**, 035109 (2001).
- ⁴⁷ E. Sasioglu, L. M. Sandratskii, P. Bruno, J. Phys.: Condens. Matter 17, 995 (2005).
- ⁴⁸ M. Rostami, M. Afkani, M. Torkamani, F. Kanjouri, Mater. Chem. Phys. **248**,122923 (2020).
- ⁴⁹ E. O'Leary, A. Ramker, D. VanBrogen, B. Dahal, E. Montgomery, S. Poddar, P. Kharel, A. Stollenwerk, and P. Lukashev, J. Appl. Phys. **128**, 113906 (2020).